ARTICLE

Dynamic Nanosurface Reconfiguration by Host-Guest Supramolecular Interactions

Received 00th January 20xx,
Accepted 00th January 20xx

DOI: 10.1039/x0xx00000x

Héctor Fernández-Caro,[a] Alejandro Méndez-Ardoy,[a,*] Javier Montenegro[a,*]

The dynamic functionalization of nanoparticle surface with biocompatible coatings is a critical step towards the development of functional nano-sized systems. While covalent approaches have been broadly exploited in the stabilization of nanoparticle colloidal systems, these strategies hinder the dynamic nanosurface chemical reconfiguration. Supramolecular strategies based on specific host-guest interactions hold promise due to their intrinsic reversibility, self-healing capabilities and modularity. Host/guest couples have recently been implemented in nanoparticle platforms for the exchange and release of effector molecules. However, the direct exchange of biocompatible hydrophilic oligomers (e.g. peptides) for the modulation of the surface charge and chemical properties of nanoparticles still remains a challenge. Here, we show the intracellular reconfiguration of nanoparticles by a host/guest mechanism with biocompatible oligomeric competitors. The surface of gold nanoparticles was functionalized with cyclodextrins hosts and the guest exchange was studied with biocompatible mono and divalent adamantyl competitors. The systematic characterization of the size and surface potential of the host/guest nanoparticles allowed the optimization of the binding and the stabilization properties of these supramolecular systems. The *in cellulo* host/guest-mediated direct reconfiguration of the peptide layer in the surface of nanoparticles is achieved by controlling the valence of adamantane-equipped peptides. This work demonstrates that host/guest supramolecular systems can be exploited for the direct exchange of pendants at the surface of nanoparticles and the intracellular dynamic chemical reconfiguration of biocompatible colloidal systems.

Introduction

The dynamic functionalization of nanoparticle surfaces constitute a critical challenge for nanosized biocompatible systems.[1,2] The chemical nature of nanoparticle surfaces can be used to control the potential coverage of biocompatible nanosystems after their incorporation in biological media.[3] Different strategies have been designed to control the assembly of nanoparticle hybrid materials that will remain stable and avoid uncontrolled aggregation or chemical decomposition.[4,5] Typically, the surface functionalization of nanoparticles is achieved by covalent anchoring strategies.[6] The formation of strong covalent bonds between nanoparticles and functional moieties is advantageous for synthesizing persistent nanocomposites with a static structure.[7] However, in most cases these nanomaterials do not show adaptive responses to the external stimuli and/or self-healing capabilities. Recent interesting strategies have probed the use of dynamic covalent exchange chemistry at the surface of stabilized nanoparticles.[8–11] A third approach builds on supramolecular interactions at the nanointerface that are generally reversible in mild conditions.[12–16] The development of stimuli-responsive supramolecular systems at the surface of nanoparticles has allowed the preparation of functional platforms for different biological applications.[17,18] In addition, nanoparticle functionalization by supramolecular interactions offers a versatile approach towards multicomponent integration into nanodevices. Particularly, the use of highly specific host-guest interactions[19] has been successfully exploited for the preparation of both soft and hard supramolecular nanosystems.[20,21]

The modularity of the host-guest approach has been widely documented with examples reporting the generation of polymer composites,[22,23] plasmonic vesicles,[24] controlled delivery[25]of antifungal[26] and anticancer drugs,[19] gene delivery[27]or the development of new biosensors.[28,29] The inclusion of multivalent host-guest recognition sites allowed the regulation of the assembly pathway, and therefore the nanostructure can be modulated by different controllable parameters, such as the ratio of the building blocks,[30,31] valency,[32] mixing regimes,[33,34] or by including stimuli responsive guests.[32,35] The reversibility of the host-guest complex can be used to trigger a release or assembly response such as the delivery of small hydrophobic molecules,[36–42]or to enable host-guest exchange. This latter strategy exploits the removal of a particular host from the nanoparticle surface after competition with an external monovalent guest of higher affinity. Such guest

[a] *Centro Singular de Investigación en Química Biolóxica e Materiais Moleculares (CIQUS), Departamento de Química Orgánica, Universidade de Santiago de Compostela, 15782 Santiago de Compostela, Spain. E-mail: alejandro.mendez@usc.es; javier.montenegro@usc.es.*

† Footnotes relating to the title and/or authors should appear here.
Electronic Supplementary Information (ESI) available: [details of any supplementary information available should be included here]. See DOI: 10.1039/x0xx00000x

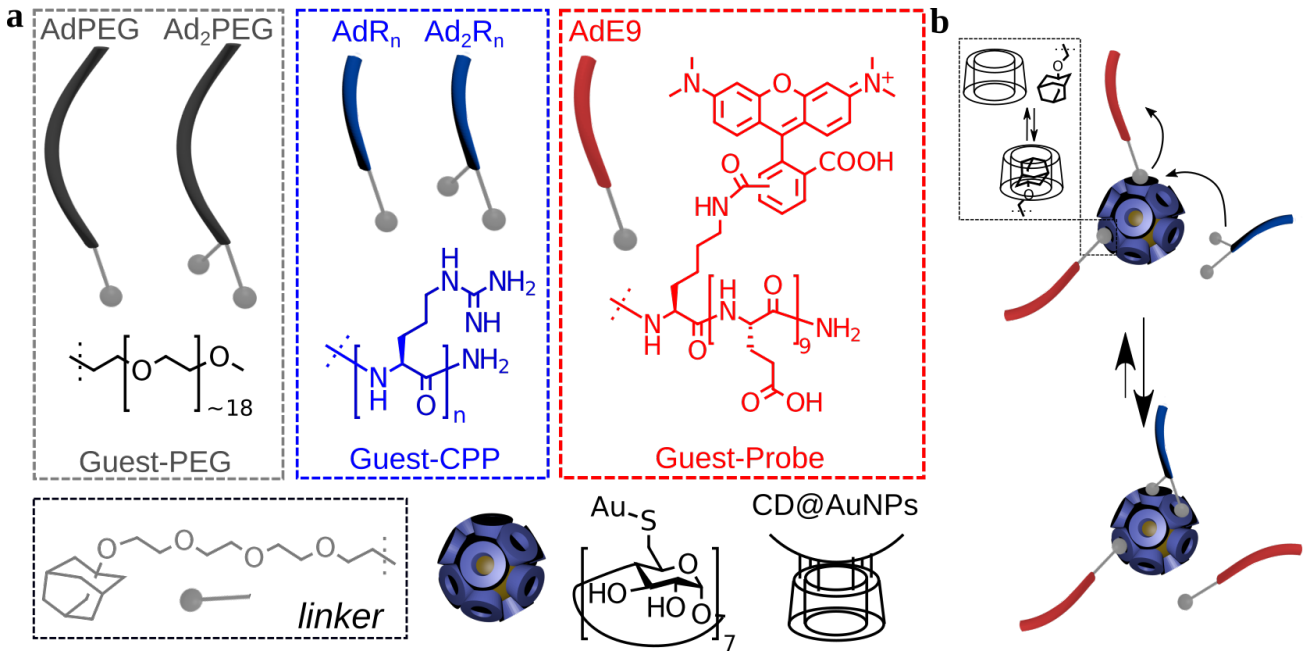

Figure 1. Schematic representation of the formation of multicomponent Peptide/PEG/*β*-CD@AuNP by combination of mono- and divalent guest molecules. a) Guest pool composed by monovalent/divalent peptides (tetra and octarginine-Ad and nonaglutamic-Ad) and polyethylene glycol (PEG) spacers. (n = 4 or 8; R and E denote arginine or glutamic amino acids respectively); b) Dynamic exchange between guests according to their valence.

exchange can be employed to provide a therapeutic effect, such as a toxic response, by using a small hydrophobic molecular guest.[43] The same strategy can further be used to regulate the catalytic activity of nanoparticles carrying a host-buried ruthenium catalyst that is activated after the addition of the specific guest.[44] These previous strategies require the inclusion of guests of differentiated affinity, which can hinder translation to cavitands where host-guest affinity constants are smaller. In addition, despite these intriguing advances in the controlled release of molecular building blocks by host/guest displacement, the intracellular dynamic reconfiguration of the surface of nanoparticles by the direct host/guest-mediated exchange of biocompatible oligomers has remained elusive. Such a direct host/guest-mediated supramolecular modulation at the nanointerface would allow the external control of the nanoparticle charge and aggregation state by exogenous biocompatible competitors of different guest valence. Here, we report the preparation and characterization of gold nanoparticles decorated with multiple copies of *β*-cyclodextrin (*β*-CD), which surface properties can be modified by direct exchange of biocompatible hydrophilic oligomers equipped with guest molecules (Adamantane, Ad). We describe a meticulous characterisation on the impact in the surface charge and the aggregation state of nanoparticle populations after their surface reconfiguration by exogenous biocompatible guests such as peptide or oligoethylene glycol pendants. Important conclusions are drawn on chemical nature and the guest valence of combinations of the guest equipped biomolecular scaffolds in competition for the nanoparticle supramolecular host. We also hypothesized that the functional dynamic guest exchange of hydrophilic biomolecules would be possible inside living cells using a suitable penetrating modulator equipped with higher valence guest. Dynamic nanoparticle surface exchange *in celullo* was demonstrated with the corresponding exogenous triggered release using guest-equipped impermeable and permeable peptide counterparts.[45]

Results and Discussion

Design

To study the host/guest direct modulation of nanoparticle surfaces, we designed and synthesized *β*-cyclodextrin functionalized nanoparticles (*β*-CD@AuNP) and adamantane (**Ad**) bearing peptides and PEG pendants. We selected the **Ad** guest due to its high binding affinity to *β*-CD hosts,[46] and a mono- and a divalent **Ad** guest motives were thus employed to adjust binding and control dynamic exchange (Fig. 1).

Preparation of guest-bearing hydrophilic peptides and stabilizers

A convergent and efficient synthetic route towards the targeted hydrophilic guests was designed based in the oxyme connection between corresponding hydrophilic pendants and the adamantane binding motif (Fig. 2). The oxyme connection was selected due to its synthetic simplicity and excellent stability at physiological conditions,[47] which gives the possibility to achieve strong molecular complexity with low synthetic effort.[48] To control and tune the selectivity of the host guest binding, monovalent (**2**) and divalent (**4**) adamantane guests were equipped with aldehydes electrophiles, which were attached via a tetraethylenglycol connector (Fig. 2). An oxidation of the corresponding alcohol[49] using Swern conditions was employed

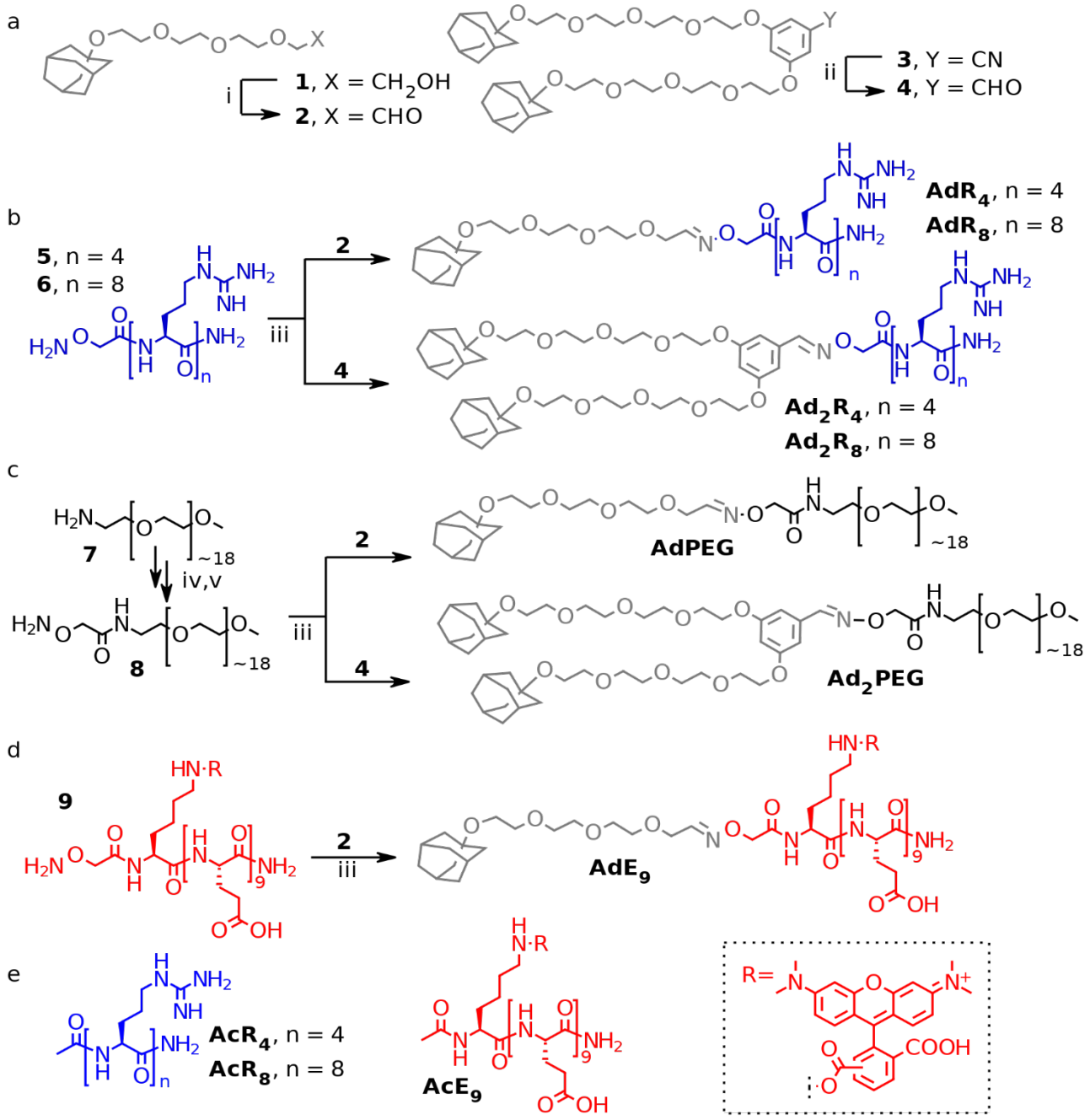

Figure 2. Synthetic scheme for the preparation of peptides and stabilizers incorporated into nanoparticles. a) Preparation of monovalent and divalent adamantane guests bearing an aldehyde function; b) preparation of polyarginine guests by condensation between alcoxyamine-bearing peptides and monovalent and divalent guests; c) preparation of polyethyleneglycol stabilizers; d) synthesis of a fluorescently labelled polyglutamic peptide bearing a monovalent guest moiety. R denotes a TAMRA fluorophore; e) control peptides used in this study. Reaction conditions: i) Oxalyl chloride, DMSO, Et_3N, DCM, -70 ºC → r.t., 28 %; ii) DIBAL-H, DCM, silica gel, -40 ºC → 0 ºC, 36 %; iii) Aldehyde, DMSO, 60 ºC, 35-19%; iv) [*tert*-butoxycarbonyl]aminoxy acetic, EDC, DIEA, DMF, r.t., 56%; v) TFA-DCM 1:1, r.t., quantitative.

to prepare the monovalent derivative **2**. Alternatively, the divalent aldehyde **4** was prepared by reduction of the nitrile precursor[49] with DIBAL-H, followed by aqueous hydrolysis. The corresponding cationic tetraarginine and octaarginine peptides (**5** and **6** respectively) and the anionic oligoglutamic peptides, bearing an alcoxyamine moiety were prepared by solid phase synthesis, N-terminated with the reactive 2-(aminooxy)acetic acid (Fig. S1a) and purified by HPLC. For the oxyme bond formation, the alkoxyamine counterparts were reacted with the different aldehydes in DMSO at 60 ºC for 2 hours, precipitated and thoroughly washed in diethyl ether to yield the monovalent **AdE_9**, **AdR_4** and **AdR_8** and the divalent **Ad_2R_4** and **Ad_2R_8** peptides

(Fig. 2b, see supporting information). The synthesis of the PEG biocompatible guests (MW ~ 800 Da) was accomplished by initial condensation between the Boc-protected alkoxyamine acetic acid to *α*-amino *ω*-methoxy PEG (**7**) followed by Boc deprotection in TFA to give **8**. The reactive PEG alcoxyamine derivative **8** was analogously coupled to aldehydes **2** and **4** to afford monovalent **AdPEG** and divalent **Ad$_2$PEG** peptide/adamantane hybrids respectively (Fig. 2c). The acetylated control peptides **AcR$_8$** and **AcE$_9$** were also prepared by standard solid-phase synthesis (Fig. 2e and Figure S1a-b). Anionic analogues of the cationic adamantane equipped peptides (**AdE$_4$**, **AdE$_8$**, **Ad$_2$E$_4$** and **Ad$_2$E$_8$**) were also prepared (Fig. S1c).

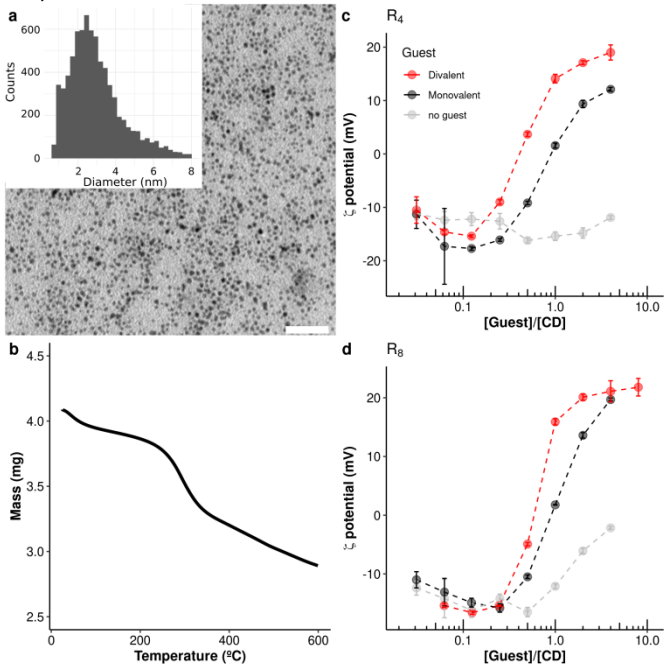

Figure 3. a) TEM micrographs of the *β*-CD@AuNP. The insert shows the size distribution obtained after image analysis. Scale bar denotes 50 nm; b) TGA experiments in O_2/N_2 atmosphere of *β*-CD@AuNP; Surface potential measurements of compounds **5**, **6**, **AdR$_4$**, **AdR$_8$**, **Ad$_2$R$_4$**, and **Ad$_2$R$_8$** in the presence of *β*-CD@AuNP at a concentration of 10 µM of *β*-CD in water; c) Evolution of nanoparticle charge upon addition of **5** (grey), **AdR$_4$** (black) and **Ad$_2$R$_4$** (red); d) Evolution of nanoparticle charge upon addition of **6** (grey), **AdR$_8$** (black) and **Ad$_2$R$_8$** (red). Error bars denote the SD of 3 replicates

Peptide particle host/guest interactions The *β*-cyclodextrin coated nanoparticles (*β*-CD@AuNPs) were prepared by following a slightly modified procedure based in the reduction of chloroauric acid (HAuCl) with $NaBH_4$ in the presence of per-thiolated *β*-cyclodextrin (See Supporting Information for details).[34] Nanoparticles were purified by repeated precipitation in acetonitrile and collection by centrifugation. TEM image analysis showed low dispersity nanoparticle size distributions of 2-3 nm as average diameter (Fig. 3a). Thermogravimetric analysis indicated about 13% of organic material (Fig. 3b), which would correspond to an average of 20 *β*-cyclodextrins covering each gold nanoparticle taking into account a diameter of 3 nm and a gold density of 19.3 g/cm^3.

The binding and exchange of guest-equipped hydrophilic biomolecules onto the surface of *β*-CD@AuNPs depends in the number of guests attached to the hydrophilic pendant and the nonspecific contribution of the electrostatic binding component. To evaluate the influence of these parameters, the *ζ*-potential of *β*-CD@AuNP nanoparticle suspensions was evaluated by titration with increasing concentrations of the oligoarginine cationic peptides (**AdR$_4$**, **Ad$_2$R$_4$**, **AdR$_8$** and **Ad$_2$R$_8$**, Fig. 3c-d). Cationic control peptides, **5** and **6**, without adamantane moieties were included to investigate the potential contribution of electrostatic interactions between the, as synthesized negatively charged *β*-CD@AuNP nanoparticles (*ζ*-potential ~ -15 mV, pH ~ 7). These control peptides (**5**, **6**) showed little or no surface potential modification at the concentration range studied, which suggested a negligible contribution of this unspecific electrostatic interactions (Fig. 3c-d, grey points). However, titration of nanoparticles with the adamantane guest-modified peptides showed the progressive *ζ*-potential increased from negative to positive values and reaching a plateau, close to +20 mV, at guest concentration of 10-50 µM. These transitions correlate with the gradual coating of the guest-equipped cationic peptides at the surface of the nanoparticle. Regardless of the length of the oligooarginine peptide, the *ζ*-potential transition was more pronounced and achieved at lower concentrations when using divalent adamantane binders (e.g. Fig. 3c, red *vs* black points). In order to estimate the nature of this interaction, we fitted the data to a simplified binding model assuming a linear relation of *ζ*-potential with peptide coverage. Thus, binding affinities of peptides to host surfaces using monovalent and multivalent thermodynamic models could be calculated (Fig. S12).[50,51]Table S1 shows the fitting parameters obtained, *K* (*β*-CD/Ad binding constant), C_{eff} the effective molarity,[51] and ζ_{max}, the maximum predicted *ζ*-potential at maximum coverage. For monovalent peptides **AdR$_4$** and **AdR$_8$**, the fitted binding constants (2.0 x 10^5 and 3.5 x 10^4 M^{-1}) correlate well to the in-solution previously reported *β*-CD/Ad binding constant (in the order of 10^5 M^{-1}).[46] Fitting of **Ad$_2$R$_4$** and **Ad$_2$R$_8$** to a multivalent model gave individual binding constants of 4.5 x 10^4 and 9.3 x 10^4 M^{-1}. The determined C_{eff} (< 0.01 M) was orders of magnitude smaller than those reported for similar divalent guests on model surfaces (0.2 M).[51] These data confirmed a robust adamantane-*β*-CD@AuNP binding, which is enhanced for the corresponding divalent guests. A dense positive charge on the particles surface can influence the host guest exchange process. For example, at high concentrations of cationic octa-arginine guests (Fig. 3d). However, charge modulation can also be controlled by adjusting the length of the peptide pendant, as shown for the tetra-arginine peptides that showed negligible effects of the cationic charge in the host/guest exchange. Binding reversibility was tested by the addition free *β*-CD to the peptide-*β*-CD@AuNP hybrid particles (Table S2). A drop in the positive *ζ*-potential of the particles, which was more pronounced for the monovalent guests, confirmed the dynamic displacement of the host/guest supramolecular equilibrium.

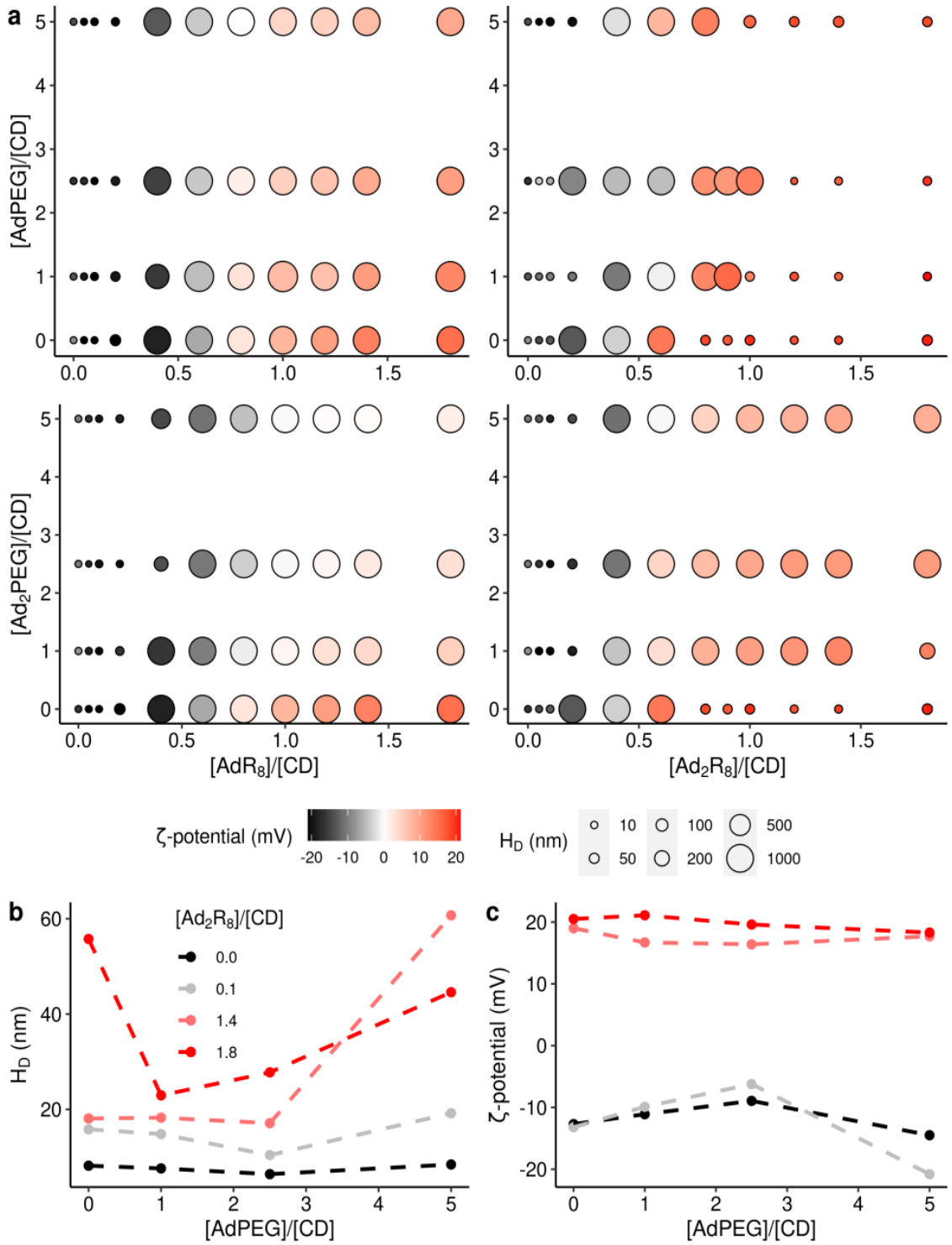

Figure 4. a) Comparative plots showing hydrodynamic diameter and nanoparticle surface potential upon the formation of multicomponent *β*-CD@AuNP (10 µM in β-CD) by combination of **AdPEG**, **Ad₂PEG**, **AdR₈** and **Ad₂R₈**. Point size is scaled to the nanoparticle size, while point fill color represents the surface potential; modulation of b) hydrodynamic diameter and c) ζ-potential of *β*-CD@AuNP (10 µM in β-CD) at different concentrations of **Ad₂R₈** and **AdPEG** in colloidal stability zones.

Host/guest dynamic nanoparticles are colloidally stabilized by developing ionic surface charge

We sought to determine the colloidal stability of the *β*-CD@AuNPs nanoparticle suspensions in the presence of guest-equipped hydrophilic conjugates in competition for the host binding sites. A detailed size and surface potential analysis of the nanoparticles was carried out in the presence of charged and neutral hydrophilic competitors such as mono or divalent guest-decorated cationic peptides and PEG oligomers (~ 700 Da). Titration experiments of colloidal suspensions of *β*-CD@AuNPs were performed in the presence of the peptide (**AdR$_8$** and **Ad$_2$R$_8$**) and the PEG (**AdPEG** and **Ad$_2$PEG**) hydrophilic pendants. The two hydrophilic guests were mixed at different molar ratios at a fixed *β*-CD concentration (in the nanoparticles surface) and equilibrated for one hour before acquiring the dynamic light scattering data (size and *ζ*-potential, Fig. 4). The results of this systematic analysis allowed us to draw several conclusions on the dependence of the guest valence and the relative competitor concentration. First, we observed two potential molar fractions areas where the *β*-CD nanoparticles remain in stable colloidal suspensions, which correspond to the addition of low equivalents of cationic peptides ([Peptide]/[CD] < 0.3, Fig. 4a, all panels), or the addition of higher amounts of divalent charged peptide **Ad$_2$R$_8$** ([Peptide]/[CD] > 1, Fig. 4a, panel top right). While in the first case little changes on surface potential are observed (*ζ* < 0), in the second a positive surface potential (> +15 mV) is reached. These "*stable zones*" are strongly correlated with a surface potential threshold of ζ < -10 mV and ζ > +15 mV (Fig. S4), and particles allocated below this threshold experienced uncontrolled aggregation. Experiments in the presence of anionic peptides (**AdE$_4$**, **AdE$_8$**, **Ad$_2$E$_4$** and **Ad$_2$E$_8$**) confirmed nanosurface host/guest exchange and stable colloidal solutions that remained stable and at negative surface potentials (> 24 hours, Fig. S6). From this data we conclude that the generation of highly charged particles in equilibrium conditions was required, although not always sufficient, to achieve colloidal stable particle suspensions. It was also confirmed that higher guest valence (di > mono) had a beneficial impact in the stabilization of the *β*-CD@AuNPs. For example, the monovalent cationic **AdR$_8$** failed to achieve particle suspension stabilization even at higher concentrations of the peptide, while increasing concentrations of **Ad$_2$R$_8$** stabilized the nanoparticle suspensions (Fig. S5a).

On the other hand, while the addition of either **AdPEG** and **Ad$_2$PEG** in the absence of polyarginine peptides yielded stable nanoparticles, mixtures of PEG and polyarginine guests tended to aggregate in most of the cases. (Fig. 4, Section S2.4). This suggests that for charged/neutral host guest couples, the ionic counterpart will take control of the stabilization process and the neutral (PEG) "*steric*" stabilization would play a minor role in these hybrid systems. Importantly, only when colloidal stabilization is achieved by electrostatic repulsion (high positive *ζ*-potential), the addition of PEG pendants could be employed to modulate the aggregation of the particle suspensions (Fig. 4b,c, extracted from values from the right top panel). For example, at a 1.8 molar ratio of divalent peptide guest *versus* cyclodextrin host, the addition of one equivalent of the monovalent polyethylene glycol ([**AdPEG**]/[CD] = 1) allows further stabilization of the colloidal suspension as shown the decrease of the size of colloidal aggregates (56 nm to 23 nm, Fig. 4b, red line). Overall, we can conclude that ionic divalent guests will have a higher affinity and thus electrostatic stabilization will prevail in host/guest colloidal hybrid systems.

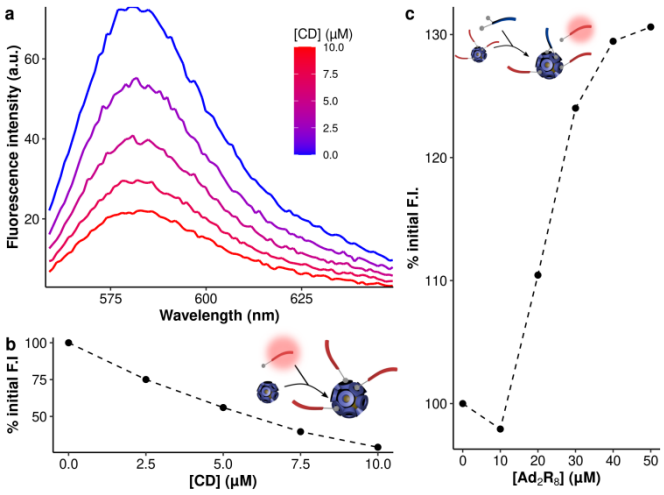

Figure 5. a) Addition of increasing concentrations of *β*-CD@AuNP to the **AdE$_9$** solution at a concentration of 10 μM. λ_{ex} = 553 nm; b) Decrease of the fluorescence at 580 nm expressed as percentage of initial intensity; c) Exchange of monovalent **AdE$_9$** by **Ad$_2$R$_8$** at peptide (CD and **AdE$_9$** concentration = 5 μM).

Dynamic Peptide Exchange at Nanoparticle Surface

An anionic oligoglutamic peptide **AdE$_9$** (Fig. 1a and 2d) equipped with a monovalent adamantane guest and a TAMRA fluorophore was designed as the counterpart to study the host/guest-mediated peptide reconfiguration at the surface of nanoparticles. In this anionic peptide (**AdE$_9$**), the fluorescent probe would be quenched/dequenched upon binding/release to the gold nanoparticles (*β*-CD@AuNPs).[39] As expected, fluorometry titrations of the **AdE$_9$** cargo with increasing amounts of *β*-CD@AuNP, resulted in a decrease of the TAMRA emission band (Fig. 5a,b). Additionally, DLS analysis of the **AdE$_9$**-*β*-CD@AuNP complexes showed a slight increase of hydrodynamic diameter (from ~ 8 to 10 nm) and a decrease of the ζ-potential (from ~ -12 to -20 mVs), which is consistent with the coating of the nanoparticle surface with the anionic peptide (Fig. S7). Host guest dynamic exchange was next studied with the **Ad$_2$R$_8$** due to the excellent binding to *β*-CD@AuNPs and the optimal kinetic colloidal stabilization of this peptide.

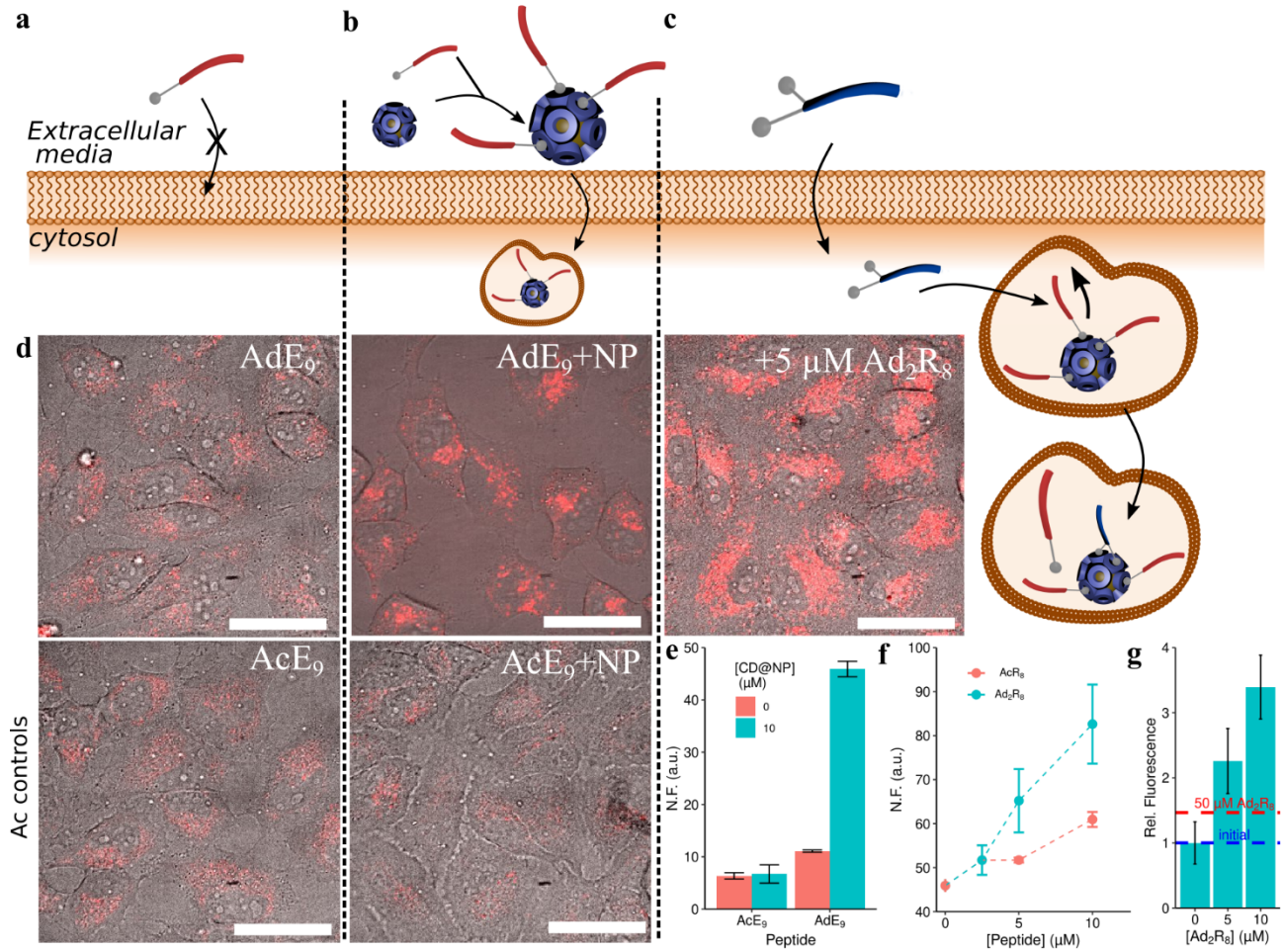

Figure 6. Intracellular guest exchange. a) bare **AdE9** (10 μM) is not uptaken by cell; b) Uptake of **AdE9** (10 μM) is trigger by the addition of *β*-CD@AuNP (10 μM in CD) to the cell medium containing the monovalent guest molecule; c) after uptake, a second divalent peptide (**Ad₂R8,** 5 μM) is added, and displaces the equilibria to the release of the first peptide inside the cell; d) Confocal images of cells after incubation with peptides **AdE9** and **AcE9** (10 μM) in the presence or absence of *β*-CD@AuNP. Scale bars denote 40 μm; e) Flow cytometry of HeLa cells populations after internalization of peptides **AdE9** (10 μM) or control peptide **AcE9** (10 μM) in the presence (blue bars) or absence (yellow bars) of *β*-CD@AuNP at a concentration of 10 μM in *β*-CD moiety. Fluorescence of control cells was substracted to all measurements; f) Cell cytometry after addition of peptide (**Ad₂R8**, blue points) and control peptide (**AcR8**, red points) to cells containing uptaken **AdE9**-*β*-CD@AuNP (10 μM). g) Exchange of **AdE₉** (10 μM) by **Ad₂R₈** at CD@AuNP (10 μM) measured by fluorescence in seeded plates. Red lines denote the relative fluorescence increase determined *in vitro* at a concentration of 50 μM (Figure 5c). In all conditions, data is plotted as an average of three wells and error bars denote their standard deviation. Dashed lines are added for eye guidance only.

Addition of the cationic **Ad₂R₈** to the preformed **AdE9**/*β*-CD@AuNP resulted in an increase of fluorescence and ζ-potential, which supports the peptide exchange and the release of the fluorescently labelled peptide from the nanoparticle surface (Fig. 5c and Fig. S8) Addition of the acetylated peptide **AcR8** did not result in fluorescence increase, which ruled out electrostatics and confirmed the specific dynamic host/guest exchange mechanism (Fig. S9). Control exchange experiments in the presence of a neutral (**Ad₂PEG**) or anionic (**Ad₂E₈**) guests revealed that the attractive-repulsive balance can influence the guest exchange when using peptide ligands of the same charge (Fig. S10a-d).

We next sought to demonstrate that direct peptide exchange at nanoparticle surfaces could be achieved inside living cells. Confocal micrographs of HeLa cells incubated with *β*-CD@AuNPs loaded with the anionic fluorescently labelled **AdE₉** peptide revealed a sizable degree of nanoparticle uptake (Fig. 6b,d). Fluorescence signal accumulated mostly in endosomes, which confirmed an energy-mediated uptake of the nanosized host/guest complex. Control experiments with the monovalent guest-equipped oligoglutamic peptide **AdE₉** in the absence of the nanoparticle platform showed a much lower internalization of the anionic peptide **AdE₉** alone in the absence of the nanoparticle carrier platform (Fig. 6a,d). Having confirmed the nanoparticle-controlled internalization of the supramolecular

Ad_2E_9 peptide/particle complexes, we decided to assay the potential dynamic exchange of the peptide guest layer inside cells by using a penetrating peptide competitor. Thus, after confirming uptake of the **Ad_2E_9**/*β*-CD@AuNP peptide**/**particle complexes, the cells were carefully washed with medium and incubated with a penetrating peptide competitor equipped with two adamantane guests (**Ad_2R_8**). A significant increase of the fluorescence signal from the nanoparticles confirmed the selective dynamic displacement of the anionic monovalent peptide guest from the surface of the internalized nanoparticles (Fig. 6c,d). A dose response dependence of the signal from the fluorescently labelled **Ad_2E_9** peptide was confirmed by confocal microscopy (Fig. 6d) and flow cytometry (Fig. 6f) with increasing concentrations of the cationic peptide competitor **Ad_2R_8**. The degree of the exchange of ligands at the surface of the nanoparticles in cells was significantly higher (by a factor of 2) than the observed for in vitro experiments (Fig. 6g). This enhanced *in cellulo* nanoparticle reconfiguration highlights the efficacy and versatility of the host/guest exchange to modulate the surface of nanoparticles in living systems. Importantly, control experiments with a penetrating peptide lacking the adamantane binding unit (**AcR_8**) did not show a fluorescence response, thus validating the host/guest-mediated peptide exchange mechanism. In addition, the corresponding MTT assays revealed negligible toxicity in all cases (Fig. S11), which ruled out any potential interference due to cytoxicity. The mechanism of uptake and the intracellular distribution of cell penetrating peptides depends on different parameters such as the cargo type/size and the peptide or the complex concentration.[53,54] The nanometric size of the particle complexes and the peptide concentrations employed here, at the low µM range, would lead to a preferential endosomal uptake (Fig. 6). However, endosomal fusion would facilitate the experimentally observed organelle localized host/guest exchange and nanoparticle reconfiguration inside cells.

Conclusions

In this work, we have experimentally demonstrated the host-guest direct exchange and reconfiguration of the surface of nanoparticles by mono and divalent guest-equipped hydrophilic biomolecular pendants. The colloidal stability of initially negatively charged host nanoparticles (*β*-CD@AuNP) was, for the first time, systematically studied in the presence of mixtures of hydrophilic biomolecular guests such as peptides and polyethylene glycol oligomers. The competition experiments allowed the identification of stability colloidal zones with a clear prevalence for the ionic (charged) and the divalent adamantane-equipped guests. The modulation of the colloidal stability of the host nanoparticles was possible by controlling the ratio between guest competitors, which allowed the modulation of the size and charge of the *β*-CD@AuNP suspensions. For example, the aggregation state and the surface potential of electrostatically stabilized cationic particle suspensions could be regulated by direct incorporation of non-charged (PEG) biocompatible pendants. The host/guest binding affinity difference between monovalent and divalent guests was exploited to promote the direct exchange inside living cells of the hydrophilic peptide at the surface of nanoparticles. To showcase nanoparticle surface reconfiguration inside cells, we employed anionic peptides, which cellular uptake was only efficiently promoted after complexation with a *β*-CD@AuNP platform. Addition of the corresponding guest-bearing penetrating peptide competitor equipped with higher valence di-adamantane guests allowed the direct intracellular exchange of the initial biomolecular peptide layer at the surface of the gold nanoparticles. Altogether, we show that guest exchange driven by multicopy guests, instead different guests, allows the dynamic reconfiguration of nanoparticles in highly complex media, driven by the selectivity of the host-guest interaction. These results establish a first experimental proof of principle of the *in cellulo* reconfiguration of nanoparticle surface by direct exchange of exogenous biocompatible oligomers (e.g. peptides) and will allow a better understanding of the fundamental forces involved in host-guest driven nanoparticle functionalization by peptides and hydrophilic pendants. This work constitutes a blueprint for the future design of future functional nanomaterials with the potential of dynamically reconfigure their surface by the direct exchange of biocompatible layers using host/guest supramolecular systems.

Experimental

Materials and methods Reagents were acquired from Fluka, Aldrich, Iris Biotech or TCI. Chemical shifts (*δ*) are reported in ppm relative to TMS (*δ* = 0). All spectra were normalized with respect the residual solvent signal. Infrared spectra were acquired in a PerkinElmer Spectrum Two ATR. Analytical HPLC was carried out in an Agilent 1260 Infinity II equipped with an Agilent SB-C18 column and connected to a 6120 Quadrupole LCMS. HR-MS was acquired in a Bruker Microtof. Derivatives **1** and **3** were prepared as described in the literature.[49]

Synthesis of *β*-CD covered gold nanoparticles (*β*-CD@AuNPs) *β*-CD@AuNPs were prepared following an adapted procedure.[34] To a solution of $HAuCl_4$ (100 mg, 255 µmol) in dry DMSO (10 mL), a solution of $NaBH_4$ (133 mg, 3.5 mmol) and per-thiol-*β*-CD[52] (33 mg, 26 µmol) in dry DMSO (10 mL) was quickly added. The reaction turned dark immediately, and the mixture was stirred overnight. Nanoparticles were precipitated by adding acetonitrile (40 mL) and the particles were collected after centrifugation,followed by washing with acetonitrile-DMSO 1:1 (40 mL, × 3), then the particles were suspended in water and freeze-dried.

Termogravimetric analysis For thermogravimetric analysis, 6-7 mg of freeze-dried *β*-CD@AuNPs were used for combustion. Samples were analysed in an TGA Q5000 (TA instruments) using the following parameters: temperature ramp: 10 °C/min; temperature range: 25–600 °C; gas flow of a mixture of air (50 mL/min) and nitrogen (10 mL/min) flow.

Dynamic Light Scattering and *ξ*-potential measurements DLS measurements were carried out in a Malvern Zetasizer Nano. Buffers were filtered through a 0.45 µm syringe filter. Size measurements were carried out with the following specification: sampling time, automatic; number of

measurements, 3 per sample; medium viscosity, 1.054 cP; scattering angle, 173 °; temperature, 25 °C. Values were given as number distribution of the major population.

Fluorescence spectroscopy experiments Fluorescence measurements were carried out in a Varian Cary Eclipse fluorescence spectrophotometer. Fluorescence spectra were acquired at 20 °C with an averaging time of 0.5 s.

Cell lines and culture HeLa cell line was maintained at 37 °C, 5% CO_2, 95 % humidity, in Dulbecco's Modified Eagle's Medium (4500 mg/L glucose, L-glutamine, sodium pyruvate and sodium bicarbonate), supplemented with 10% fetal bovine serum and 1% of Penicillin-Streptomycin-Glutamine Mix, and kept in an INCO108 incubator (Memmert).

Cell uptake and exchange experiments HeLa cells seeded the day before on glass bottom dishes were washed with DMEM (Dulbecco's Modified Eagle's Medium (DMEM, 4500 mg/L glucose, L-glutamine, sodium pyruvate and sodium bicarbonate) without serum, antibiotics and phenol red and incubated for 30 min with 10 μM CD@AuNPs in combination with 10 μM of guest-anchored peptide in DMEM. This solution was removed and cells were washed two times with DMEM. Then, cells were incubated for another 30 min with the peptide in DMEM at the concentrations indicated in the corresponding Fig. Later, cells were washed once with DMEM and examined on the confocal microscope.

Flow cytometry HeLa cells, seeded the day before at 10.000 cells/well of a 96-well plate, were treated for 30 min with the preformed complex of 10 μM of CD@AuNPs and 10 μM of **AdE_9** diluted in DMEM without serum, antibiotics and phenol red. Cells were then washed (2 ×) with DMEM and incubated with the divalent peptide (**Ad_2R_4** and **Ad_2R_8**) during 30 min at the different concentrations in DMEM at 37 °C. After the incubation, cells were washed with DMEM and trypsinized.

As controls, 10 μM *β*-CD@AuNP in the presence or absence of 10 μM **AdE_9** or **AcE_9** diluted in DMEM were also performed. After 60 min of incubation, cells were washed with DMEM and trypsinized. Trypsin was neutralized with 2 % FBS in PBS with 5 mM EDTA and cell fluorescence was measured on a Guava EasyCyteTM(millipore) cytometer using a green laser (532 nm) collecting the emission at 575/25 nm (TAMRA).

Cells with typical FSC and SSC parameters were selected and the median fluorescence intensity (MFI) calculated for each sample. Each condition was done 4 times. In all cases, data analysis was performed with InCyte software included in GuavaSoft 3.2 (Millipore).

Toxicity quantification by MTT assays To evaluate the toxicity of the treatment of cells with *β*-CD@AuNP (10 μM) and **AdE_9** (10 μM) and the following incubation with the different peptides in DMEM without serum, antibiotics and phenol red. HeLa cells were submitted to an MTT assay 1 hour after the incubation. One day before the assay, a suspension of HeLa were plated in 96-well tissue culture plates by adding 100 μL (10.000 cells) per well. The day after, the medium was removed and cells were incubated in DMEM in the presence of different conditions at different concentrations (50 μL/well) during 1 hour of incubation at 37 °C. After the incubation, DMEM with the compounds was removed, pre-warmed DMEM containing 10 % FBS and MTT (5 mg/mL in PBS, 10 μL/well) was added to the wells and the cells were further incubated for 2 h. Supernatant was carefully removed and the water-insoluble formazan salt was dissolved in DMSO (100 μL/well). The absorbance at 570 nm was measured with an Infinite F200Pro Plate reader. Data points were collected 4 times and expressed as normalized values for untreated as control cells (100%) after blank subtraction.

Conflicts of interest

There are no conflicts to declare.

Acknowledgements

This work was partially supported by the Spanish Agencia Estatal de Investigación (AEI) [SAF2017-89890-R, CTQ2014-59646-R and CTQ2016-78423-R], the Xunta de Galicia (ED431G/09, ED431C 2017/25 and 2016-AD031) and the ERDF. H. F.-C. received a predoctoral fellowship (Xunta de Galicia, ED481A-2017/047). A. M.-A. received a MCIF from the EC (GLYCONANOPEP-750248). J. M. holds a Ramón y Cajal (RYC-2013-13784), an ERC-Stg (DYNAP-677786) and a Young Investigator Grant from the HFSP (RGY0066/2017).

Notes and references

1 J. K. Patra, G. Das, L. F. Fraceto, E. V. R. Campos, M. del P. Rodriguez-Torres, L. S. Acosta-Torres, L. A. Diaz-Torres, R. Grillo, M. K. Swamy, S. Sharma, S. Habtemarian and H.-S. Shin, *J. Nanobiotechnol.*, 2018, **16**, DOI:10.1186/s12951-018-0392-8.

2 D. Bobo, K. J. Robinson, J. Islam, K. J. Thurecht and S. R. Corrie, *Pharm. Res.*, 2016, **33**, 2373–2387.

3 P. M. Kelly, C. Åberg, E. Polo, A. O'Connell, J. Cookman, J. Fallon, Ž. Krpetić and K. A. Dawson, *Nat. Nanotechnol.*, 2015, **10**, 472–479.

4 R. Mout, D. F. Moyano, S. Rana and V. M. Rotello, *Chem. Soc. Rev.*, 2012, **41**, 2539-2544.

5 G. Chen, K. J. Gibson, D. Liu, H. C. Rees, J.-H. Lee, W. Xia, R. Lin, H. L. Xin, O. Gang and Y. Weizmann, *Nat. Mater.*, 2018, **18**, 169–174.

6 R. A. Sperling and W. J. Parak, *Phil. Trans. R. Soc. A*, 2010, **368**, 1333–1383.

7 C. L. Schreiber and B. D. Smith, *Nat. Rev. Chem.*, 2019, **3**, 393–400.

8 M. Diez-Castellnou, R. Suo, N. Marro, S. A. L. Matthew and E. R. Kay, *Chem. Eur. J.*, 2021, **27**, 9948–9953.

9 W. Edwards, N. Marro, G. Turner and E. R. Kay, *Chem. Sci.*, 2018, **9**, 125–133.

10 F. della Sala and E. R. Kay, *Angew. Chem. Int. Ed.*, 2015, **54**, 4187–4191.

11 N. Marro, F. Della Sala and E. R. Kay, *Chem. Sci.*, 2020, **11**, 372–383.

12 P. J. de Vink, T. van der Hek and L. Brunsveld, *Chem. Sci.*, 2021, **12**, 6726–6731.

13 D. E. Clarke, G. Wu, C. Wu and O. A. Scherman, *J. Am. Chem. Soc.*, 2021, **143**, 6323–6327.

14 K. l. Assaf and W. M. Nau, *Chem. Soc. Rev.*, 2015, **44**, 394–418.

15 G. Gil-Ramírez, A. Shah, H. El Mkami, K. Porfyrakis, G. A. D. Briggs, J. J. L. Morton, H. L. Anderson and J. E. Lovett, *J. Am. Chem. Soc.*, 2018, **140**, 7420–7424.

16 H. Fernández-Caro, I. Lostalé-Seijo, M. Martínez-Calvo, J. Mosquera, J. L. Mascareñas and J. Montenegro, *Chem. Sci.*, 2019, **10**, 8930–8938.
17 M. J. Webber, E. A. Appel, E. W. Meijer and R. Langer, *Nat. Mater.*, 2016, **15**, 13–26.
18 M. J. Webber and R. Langer, *Chem. Soc. Rev.*, 2017, **46**, 6600–6620.
19 Y.-F. Chen, Y.-H. Wang, C.-S. Lei, C. A. Changou, M. E. Davis and Y. Yen, *J. Biomed. Sci.*, 2019, **26**, DOI:10.1186/s12929-019-0583-0.
20 V. Montes-García, J. Pérez-Juste, I. Pastoriza-Santos and L. M. Liz-Marzán, *Chem. Eur. J.*, 2014, **20**, 10874–10883.
21 R. Mejia-Ariza, L. Graña-Suárez, W. Verboom and J. Huskens, *J. Mater. Chem. B*, 2017, **5**, 36–52.
22 R. J. Coulston, S. T. Jones, T.-C. Lee, E. A. Appel and O. A. Scherman, *Chem. Commun.*, 2011, **47**, 164–166.
23 G. Osman, J. Rodriguez, S. Y. Chan, J. Chisholm, G. Duncan, N. Kim, A. L. Tatler, K. M. Shakesheff, J. Hanes, J. S. Suk and E. J. Dixon, *J. Control. Release*, 2018, **285**, 35–45.
24 W. C. de Vries, M. Niehues, M. Wissing, T. Würthwein, F. Mäsing, C. Fallnich, A. Studer and B. J. Ravoo, *Nanoscale*, 2019, **11**, 9384–9391.
25 Y. Lu, W. C. de Vries, N. J. Overeem, X. Duan, H. Zhang, H. Zhang, W. Pang, B. J. Ravoo and J. Huskens, *Angew. Chem. Int. Ed.*, 2018, **58**, 159–163.
26 F. Wang, P. Yang, J. Choi, P. Antovski, Y. Zhu, X. Xu, T.-H. Kuo, L.-E. Lin, D. N. H. Kim, P.-C. Huang, H. Xu, C.-F. Lee, C. Wang, C.-C. Hsu, K. Chen, P. S. Weiss and H.-R. Tseng, *ACS Nano*, 2018, **12**, 6851–6859.
27 L. Gallego-Yerga, J. M. Benito, L. Blanco-Fernández, M. Martínez-Negro, I. Vélaz, E. Aicart, E. Junquera, C. Ortiz Mellet, C. de llarduya and J. M. García Fernández, *Chem. Eur. J.*, 2018, **24**, 3825–3835.
28 L. He, X. Yang, F. Zhao, K. Wang, Q. Wang, J. Liu, J. Huang, W. Li and M. Yang, *Anal. Chem.*, 2015, **87**, 2459–2465.
29 P. Wang, C. Zhang, H.-W. Liu, M. Xiong, S.-Y. Yin, Y. Yang, X.-X. Hu, X. Yin, X.-B. Zhang and W. Tan, *Chem. Sci.*, 2017, **8**, 8214–8220.
30 H. Wang, S. Wang, H. Su, K.-J. Chen, A. L. Armijo, W.-Y. Lin, Y. Wang, J. Sun, K. Kamei, J. Czernin, G. R. Caius and H.-R. Tseng, *Angew. Chem. Int. Ed.*, 2009, **48**, 4344–4348.
31 L. Graña-Suárez, W. Verboom, T. Buckle, M. Rood, F. W. B. van Leeuwen and J. Huskens, *J. Mater. Chem. B*, 2016, **4**, 4025–4032.
32 C. Stoffelen, E. Staltari-Ferraro and J. Huskens, *J. Mat. Chem. B*, 2015, **3**, 6945–6952.
33 C. Stoffelen, J. Voskuhl, P. Jonkheijm and J. Huskens, *Angew. Chem. Int. Ed.*, 2014, **53**, 3400–3404.
34 R. Mejia-Ariza and J. Huskens, *J. Mater. Chem. B*, 2014, **2**, 210–216.
35 H. Yao, M. Qi, Y. Liu and W. Tian, *Chem. Eur. J.*, 2016, **22**, 8508–8519.
36 Y. Zhao, Y. Huang, H. Zhu, Q. Zhu and Y. Xia, *J. Am. Chem. Soc.*, 2016, **138**, 16645–16654.
37 M. S. Ahmed, C. B. Rodell, M. Hulsmans, R. H. Kohler, A. D. Aguirre, M. Nahrendorf and R. Weissleder, *Bioconjugate Chem.*, 2019, **30**, 733–740.
38 Y. Shi, J. Goodisman and J. C. Dabrowiak, *Inorg. Chem.*, 2013, **52**, 9418–9426.
39 C. Park, H. Youn, H. Kim, T. Noh, Y. H. Kook, E. T. Oh, H. J. Park and C. Kim, *J. Mater. Chem.*, 2009, **19**, 2310.
40 W.-H. Chen, Q. Lei, G.-F. Luo, H.-Z. Jia, S. Hong, Y.-X. Liu, Y.-J. Cheng and X.-Z. Zhang, *ACS Appl. Mater. Inter.*, 2015, **7**, 17171–17180.
41 D. N. Heo, D. H. Yang, H.-J. Moon, J. B. Lee, M. S. Bae, S. C. Lee, W. J. Lee, I.-C. Sun and I. K. Kwon, *Biomaterials*, 2012, **33**, 856–866.
42 A. Aykaç, M. C. Martos-Maldonado, J. M. Casas-Solvas, I. Quesada-Soriano, F. García-Maroto, L. García-Fuentes and A. Vargas-Berenguel, *Langmuir*, 2013, **30**, 234–242.
43 C. Kim, S. S. Agasti, Z. Zhu, L. Isaacs and V. M. Rotello, *Nat. Chem.*, 2010, **2**, 962–966.
44 G. Y. Tonga, Y. Jeong, B. Duncan, T. Mizuhara, R. Mout, R. Das, S. T. Kim, Y.-C. Yeh, B. Yan, S. Hou and V. M. Rotello, *Nat. Chem.*, 2015, **7**, 597–603.
45 P. M. Fischer, *Med. Res. Rev.*, 2007, **27**, 755–795.
46 M. V Rekharsky and Y. Inoue, *Chem. Rev.*, 1998, **98**, 1875–1918.
47 J. Kalia and R. T. Raines, *Angew. Chem. Int. Ed.*, 2008, **47**, 7523–7526.
48 C. Gehin, J. Montenegro, E.-K. Bang, A. Cajaraville, S. Takayama, H. Hirose, S. Futaki, S. Matile and H. Riezman, *J. Am. Chem. Soc.*, 2013, **135**, 9295–9298.
49 A. Mulder, S. Onclin, M. Péter, J. P. Hoogenboom, H. Beijleveld, J. ter Maat, M. F. García-Parajó, B. J. Ravoo, J. Huskens, N. F. van Hulst and D. Reinhoudt, *Small*, 2004, **1**, 242–253.
50 J. Huskens, L. J. Prins, R. Haag and J. Ravoo, *Multivalency: Concepts, Research and Applications*, Wiley, 2018.
51 J. Huskens, A. Mulder, T. Auletta, C. A. Nijhuis, M. J. W. Ludden and D. N. Reinhoudt, *J. Am. Chem. Soc.*, 2004, **126**, 6784–6797.
52 M. T. Rojas, R. Koeniger, J. F. Stoddart and A. E. Kaifer, *J. Am. Chem. Soc.*, 1995, **117**, 336–343.
53 M. Hällbrink, J. Oehlke, G. Papsdorf and M. Bienert, *Biochim. Biophys. Acta - Biomembr.*, 2004, **1667**, 222–228.
54 M. Pazo, G. Salluce, I. Lostalé-Seijo, M. Juanes, F. González, R. Garcia-Fandiño and J. Monetenegro, *RSC Chem. Biol.* 2021, **2**, 503-512.